# Nonequilibrium behavior of the Pb wetting layer on Si(111)7×7

M. W. Gramlich,[1] S. T. Hayden,[1] Yiyao Chen,[1] C. Kim,[2] E. H. Conrad,[3] M. C. Tringides,[4] and P. F. Miceli[1]

[1]*Department of Physics and Astronomy, University of Missouri-Columbia, Columbia, Missouri 65211, USA*

[2]*Department of Physics and Research Institute for Basic Sciences, Kyung Hee University, 1 Hoeki-dong, Dongdaemoon-gu, Seoul 130-701, Korea*

[3]*The Georgia Institute of Technology, Atlanta, Georgia 30332-0430, USA*

[4]*Department of Physics and Astronomy, Iowa State University, Ames, Iowa 50011, USA*

(Received 22 November 2010; revised manuscript received 20 May 2011; published 8 August 2011)

The growth and stability of the Pb8×8 wetting layer on Si(111)7×7, which provides a foundation for growing quantum-size-effect nanocrystals, was investigated by *in situ* x-ray scattering. Our experimental results reveal that the wetting-layer structure evolves temporally over a remarkably broad range of temperatures and that there are *two* distinct temperature regimes of nonequilibrium behavior. When grown at lower temperature (below 170 °C), it was discovered that the wetting-layer structure changes with time, indicating that its disordered structure is not static; annealing in this regime improves the order of the wetting layer. Growth at higher temperature (170 °C $< T <$ 250 °C), however, leads to a time-dependent degradation of the 8×8 structure due to the deterioration of the underlying Si(111)7 × 7. Thermal measurements determined an activation energy of 0.4 eV in the low-temperature regime, whereas in the high-temperature regime, a two-step process is observed, which has activation energies of approximately 1.3 and 1.9 eV. The results provide important considerations for understanding the anomalous kinetic behavior of quantum-size-effect Pb nanocrystals on Si(111)7×7, which is facilitated by the wetting layer.

DOI: 10.1103/PhysRevB.84.075433 PACS number(s): 68.35.−p, 68.60.Dv, 68.55.−a

## I. INTRODUCTION

In the pursuit to understand the growth and formation of nanoscale materials, it has been realized that their reduced physical dimensions can also lead to novel growth behavior. An important example is given by metallic nanocrystals grown on semiconductor substrates, where the geometrical confinement of the conduction electrons can affect the overall energy of the nanocrystal.[1] Indeed, quantum size effects (QSE) have been observed in metallic islands, which exhibit certain "magic heights" of atomic layers.[2,3]

Because epitaxial crystal growth is usually dominated by kinetic limitations,[4] the equilibrium nature of the growth implied by QSE is unexpected. Experiments on Pb/Si(111)7×7, however, have shown that the growth kinetics are anomalously fast, thereby providing some rationale for achieving the magic heights.[5] The origin of the fast kinetics is still unknown, but the region between the nanocrystals *must* facilitate fast mass transport. For this reason, we are interested in understanding the structure of the wetting layer that exists in the region between the Pb nanoislands.

Depositing Pb on Si(111)7×7 follows a Stranski-Krastanov growth mode whereby the Pb completely wets the substrate with a layer (the "wetting layer") that is one monolayer in thickness, followed by the formation of islands (the QSE islands) for higher coverage.[6] Previous surface x-ray diffraction investigations into the structure of the wetting layer have found that it forms a highly disordered 8×8 structure that is commensurate with the Si(111)7×7 unit cell.[7] Unfortunately, a complete structural determination was hindered by the disorder within the wetting layer, a limited data set, and by the fact the measurements were performed for a coverage of $\backsim$2 ML, where the surface was significantly covered by islands. STM studies on the Pb/Si(111)7×7 wetting layer have been complicated by an inability to resolve individual Pb atoms in the structure,[8] and several structures have been proposed based on the limited resolution images.[8,9] Recent x-ray scattering studies have shown that, surprisingly, the portion of the wetting layer directly beneath the islands is transformed to face-centered-cubic (fcc) Pb so that the islands consume the wetting layer.[10,11] The material remaining between the islands, however, continues to exist in the wetting-layer structure. Another important complication, as revealed in this paper, is that the wetting-layer structure also changes with time because it is not in equilibrium. Therefore, the detailed structure of the Pb8×8 wetting layer is still left as an open question.

The Pb8×8/Si(111)7×7 wetting layer is known to be metastable because the presence of the metal negates the need for the dimerization that drives the Si(111)7×7 reconstruction. Annealing above 200 °C destroys the Pb/Si(111)7×7 and the surface reorders into a Pb/Si(111)1×1.[12,13] Upon cooling, for coverages around 1 ML, the system orders in the $\alpha$ phase, which refers to a collection of closely related surface structures based on a Pb$\sqrt{3} \times \sqrt{3}$/Si(111) structure.[14] The system exhibits a complex phase diagram that has been shown to derive from large commensurate unit cells that are constructed from combinations of $\sqrt{3} \times \sqrt{3}$ and $\sqrt{7} \times \sqrt{3}$ units.[15]

In this paper, we show that the wetting layer is unstable in *two* temperature regimes and our results reveal that the structure of the wetting layer evolves temporally over a remarkably broad range of temperatures due to the fact that there are two physically independent causes of the instability. When grown at lower temperature, the initial wetting layer is found to slowly anneal into a *more-ordered structure*, which suggests that the wetting layer is highly dynamic as it attempts to accommodate the large corrugation of the Si(111)7×7 substrate. At higher temperature, the wetting-layer structure is found to slowly *degrade* with time, consistent with the

 

above-mentioned impending destruction of the Si(111)7×7 reconstruction. These effects occur on typical laboratory time scales over a broad temperature range, from below 0 °C to over 200 °C.

## II. EXPERIMENTAL DETAILS

X-ray scattering experiments were performed *in situ* using the surface scattering chamber (base pressure of $1 \times 10^{-10}$ Torr) on a Psi diffractometer located at the 6IDC beam line at the Advanced Photon Source. The photon energy was 12.4 keV and the data were collected using a Bicron detector. We will use hexagonal coordinates $(H,K,L)_H$ to describe the reciprocal lattice of Si, which is defined by the following relationship between hexagonal $(H)$ and cubic $(C)$ coordinates: $a_H = \frac{a_C}{\sqrt{2}}$ and $c_H = \sqrt{3}a_C$, where $a_C = 0.54305$ nm is taken as the room-temperature Si cubic lattice constant and $[0,0,3]_H = [1,1,1]_C$ is along the surface normal direction.

The commercially available 1-mm-thick *n*-type Si(111) substrates used in these studies had a resistivity in the range of 1-10 Ωcm. Surface miscut angles were determined to be in the range of 0.015°–0.05° by x-ray reflectivity. The Si(111)7×7 surface was prepared by heating the Si(111) substrate to 1200 °C for ∽1 min and then slowly cooling from 1000 °C over ∽10 min to obtain the reconstructed surface. The quality of the surface was determined by transversely scanning the $(\frac{8}{7},0,0.1)_H$ in-plane reflection, which will be referred to as $(\frac{8}{7},0)_H$. It exhibited an angular width in the range of 0.02°–0.05°, which corresponds to domain sizes in the range of 8000–3300 Å. This large domain size is on the order of the step length given by the surface miscut angle and was routinely observed for all surfaces that were prepared as described above.

Pb was deposited on the clean Si(111)7×7 surface from a crucible that was heated by an electron beam with flux feedback (Omicron EFM). Two standard deposition rates, 0.25 ML/min and 0.5 ML/min, were used where 1 ML is measured in $Pb(111)_C$ units (1 ML = $9.43 \times 10^{14}$ atoms/cm$^2$). The deposition rates were calibrated by measuring the rate of intensity oscillations with coverage (for high coverage, >10 ML, and $T \backsim 100$ K) at the Pb specular anti-Bragg position ($L = 1.64$), with each oscillation period corresponding to the completion of two Pb(111) layers.[16] The uncertainty and reproducibility of the coverage is estimated to be ±0.1 ML. The sample was cooled to a minimum temperature of 100 K using a He closed-cycle refrigerator. Heating for the purpose of preparing the Si(111)7×7 was performed by electron bombardment, whereas maintaining the temperature during the scattering measurements (−50 °C to 450 °C) utilized radiative heating from the tungsten filament behind the sample. The temperature was measured by a type-*K* thermocouple connected to the bottom of the sample holder, which was also used for temperature control with a feedback system. The thermal stability during measurements was ±0.5 °C and the absolute temperature accuracy was better than ±10 °C.

## III. RESULTS AND DISCUSSION

The intriguing behavior of the wetting layer is displayed in Fig. 1, which shows the normalized $(\frac{8}{7},0)_H$ intensity measured

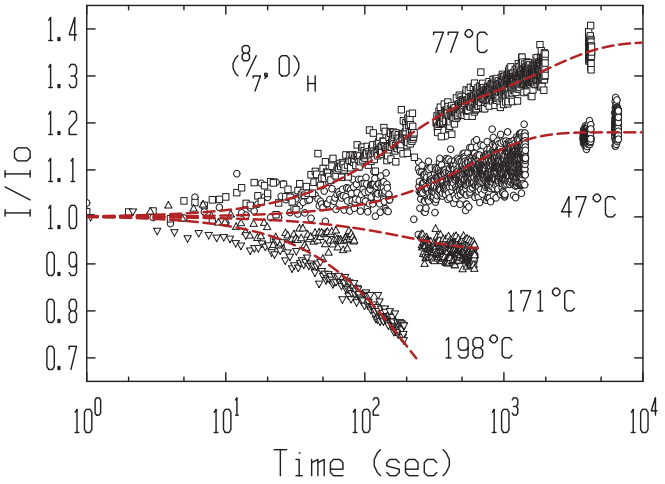


FIG. 1. (Color online) The $(\frac{8}{7},0)_H$ peak intensity measured with elapsed time after depositing 1.2 ML of Pb at different fixed substrate temperatures. The intensity has been normalized by the initial peak intensity $I_0$ measured immediately after (∽1 s) deposition. As can be seen, there are two regimes of time dependence: low-temperature and high-temperature regimes, which exhibit increasing or decreasing intensity with time, respectively. The dashed curves represent fits to the data, as described in the text.

as a function of elapsed time after depositing 1.2 ML of Pb on Si(111)7×7 at different temperatures. The $(\frac{8}{7},0)_H$ reflection represents the fundamental periodicity of the Pb8×8 wetting layer and, therefore, it is a good indicator of the overall order of the wetting layer. The intensity is normalized by the initial intensity $I_0$, which was measured immediately after (∽1 s) deposition. As can be seen, not only is there a substantial change of intensity with the elapsed time, indicating that the wetting layer is not in equilibrium, but there also exist two *oppositely behaving* annealing regimes: a lower-temperature regime where the intensity is observed to *increase* with time, and a higher-temperature regime where the intensity *decreases* with time. Moreover, the rate of annealing increases with increasing temperature in *both* temperature regimes; although, annealing in the lower-temperature regime is expected to eventually give way to a transition to the higher-temperature regime. These two temperature regimes are also apparent in Fig. 2, which shows the temperature dependence of the initial intensity. The intensity increases more than tenfold with increasing deposition temperature from −50 °C to 170 °C, followed by a precipitous decrease for higher growth temperatures, above ∽200 °C.

Similar results are essentially obtained by depositing at a lower temperature and then annealing at a higher temperature. Figure 3(a) shows the integrated intensity of the $(\frac{8}{7},0)_H$ reflection for a 1.2-ML film that was deposited at −20 °C and then annealed in successive ∽10-min steps at the given temperatures. It can be seen that the general trend of increasing intensity with annealing temperature is observed, although, the intensity increase is somewhat less than in Fig. 2. Therefore, equivalent results can be obtained in three ways: by annealing with time or temperature, or by depositing at a higher temperature.

The increasing intensity of the $(\frac{8}{7},0)_H$ reflection indicates that the as-deposited wetting layer is not an equilibrium

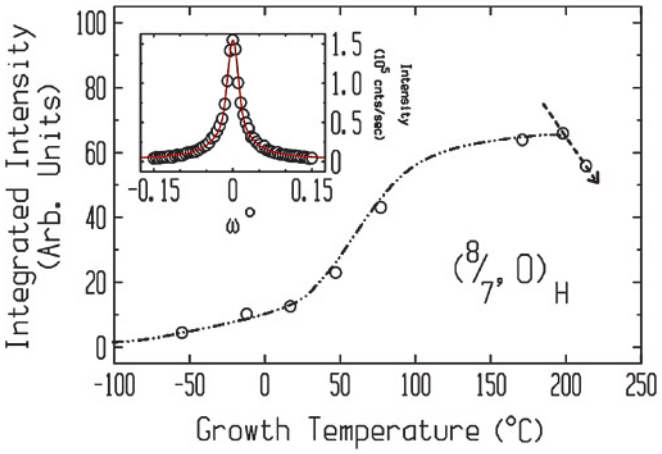


FIG. 2. (Color online) The $(\frac{8}{7},0)_H$ transversely integrated intensity (obtained from scans similar to the one shown in the inset) for 1.2 ML of Pb deposited at different fixed substrate temperatures. These intensities were measured shortly after ($\backsim$1 min) deposition. The dashed-dotted curve through the data is a "guide to the eye." The dashed arrowed line indicates the beginning of the decaying intensity process that was also observed in Fig. 1.

structure and, moreover, this evolution corresponds to an improving atomic-scale order within the unit cell, as we will now discuss. Figure 4 shows, for many fractional order $(\frac{m}{7},\frac{n}{7})_H$ surface reflections, the ratio of the intensity measured on an annealed sample to the initial intensity of the as-grown Pb wetting layer at −45 °C. This was measured both during and after annealing. Ratios that are greater than unity correspond to intensities that increased during annealing, whereas ratios

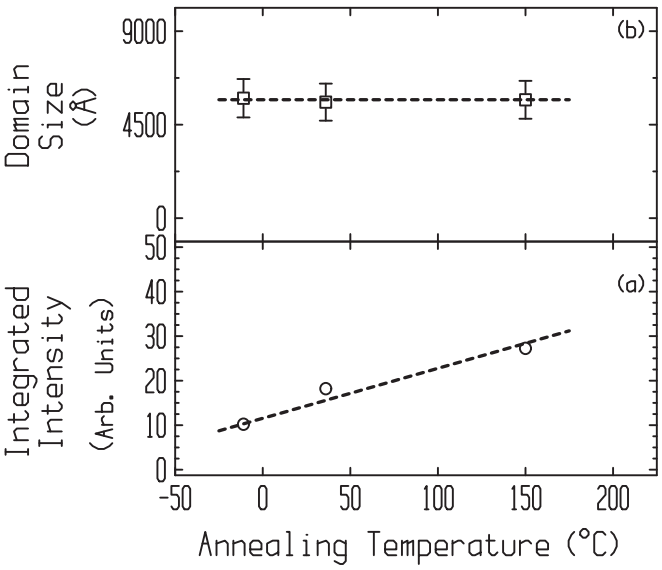


FIG. 3. The evolution of the $(\frac{8}{7},0)_H$ reflection as a function of annealing temperature (within the low-temperature regime). 1.2 ML of Pb was deposited at −20 °C and annealed in 10-min steps at the given temperatures. (a) The integrated intensity increases with annealing temperature, indicating the improved ordering within the Pb8 × 8 unit cell as the temperature increases. (b) The domain size, which was determined from the transverse width of the reflection, does not change during annealing.

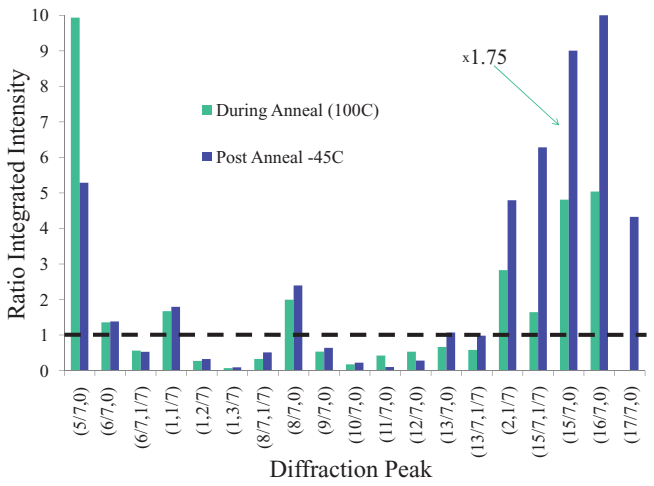


FIG. 4. (Color online) The intensity ratios of different diffraction peaks $(H,K)_H$ of a 1.2-ML Pb film are shown for two cases of annealing: one measured at the annealing temperature of 100 °C ($\backsim$1 h) and one measured after cooling to −45 °C. The intensity ratio is defined as the intensity of the annealed wetting layer divided by the intensity of the as-deposited wetting layer at −45 °C. The horizontal dashed line at a ratio of unity demarks the level of change: An intensity ratio less than unity indicates a reflection that weakens with annealing, whereas a ratio greater than unity indicates a strengthening of the reflection. Note that the intensity ratio for the $(\frac{15}{7},0)_H$ was reduced by a factor of 1.75 because its large change skews the other peaks.

less than unity correspond to intensities that decreased during annealing. The graph strikingly shows that some peaks grow while others decrease, clearly indicating that the atomic-scale structure within the Pb8×8 unit cell was changed by annealing. Note that the increasing intensity observed in Figs. 1–3 is *not* due to an increasing surface fraction because the domain size does not change [see Fig. 3(b)]. Additionally, there is an approximate pattern to the intensity changes in Fig. 4 : Reflections that are in the vicinity of integer multiples of $\frac{8}{7}$ tend to increase with annealing, whereas the others decrease (an undistorted 8×8 would have peaks only at integer multiples of $\frac{8}{7}$). The peaks that increase are typically the stronger intensities, while the ones that decrease are weaker. The only exception is the $(\frac{5}{7},0)$, which has very low intensity; however, this does not change the overall trend. Figure 4 also reveals that there is an additional intensity increase at these positions as the sample is cooled after annealing, indicating the effect of a strong thermal Debye-Waller factor. These results, therefore, demonstrate that the ordering within the unit cell *improves* upon annealing.

Turning now to the higher temperature annealing in Fig. 1, we see that the opposite temperature dependence is observed. As discussed in the Introduction, it is known that annealing at elevated temperatures leads to the destruction of the underlying Si(111)7×7 surface that gives way to Pb/Si(111)-1×1 structure and, upon cooling, it transforms to the $\alpha$-phase Pb/Si(111). Figure 5 shows that, indeed, after annealing above 200 °C and subsequently cooling, the expected[7,13,15,20] reflection at approximately $(\frac{2}{3},\frac{2}{3})_H$ for the $\alpha$ phase appears. Therefore, the precipitous drop in intensity with temperature above 200 °C in Fig. 2 as well as the slow intensity decay above 170 °C in Fig. 1

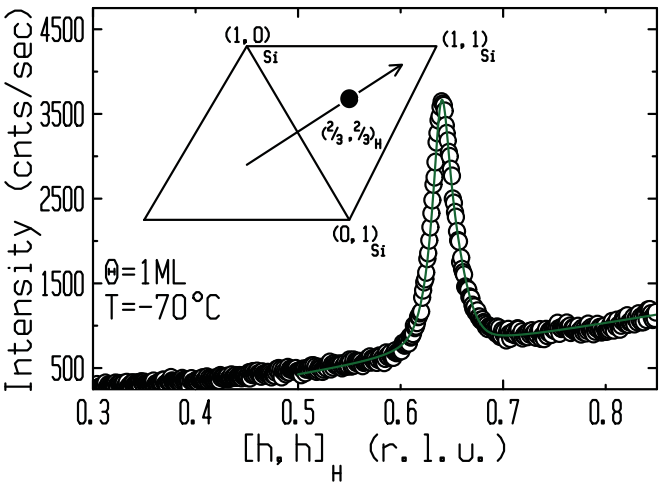


FIG. 5. (Color online) An $[h,h]_H$ scan shows that annealing 1 ML of Pb above 200 °C and cooling to −70 °C produces the main Bragg reflection of the $\alpha$ phase. Therefore, the intensity decay observed in Fig. 1 relates to the destruction of the Pb/Si(111)7×7, which leads to the $\alpha$ phase upon cooling. The solid curve is a Gaussian and background that was fit to the data. The inset schematically shows the hexagonal reciprocal lattice with the direction of the scan.

are due to the Pb-induced destruction of the Si(111)7×7. This is further corroborated by the inset to Fig. 6 that demonstrates a decreasing surface fraction of Pb8×8 during annealing: The measured surface reflections exhibit the *same* relative intensity decay, which is in sharp contrast to the lower-temperature annealing results in Fig. 4, where some peaks increase while others decrease.

The decaying intensity observed at the higher temperatures in Fig. 1 was investigated in more detail by measuring over a longer period of time and over a larger temperature range, as

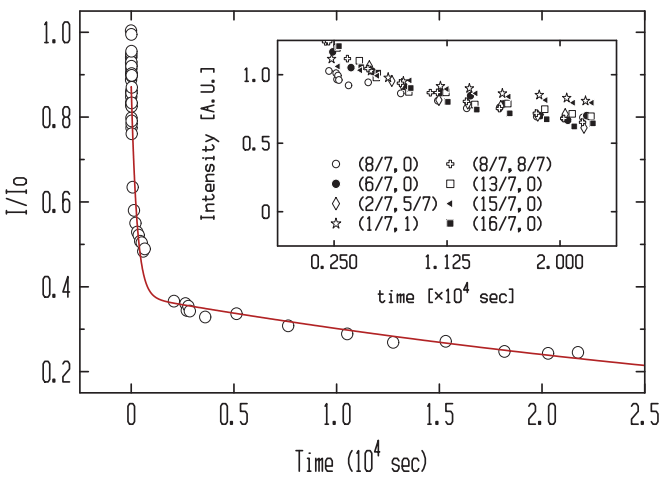


FIG. 6. (Color online) The $(\frac{8}{7},0)_H$ peak intensity, normalized to $I_0$, measured as a function of elapsed time after 1.2 ML of Pb was deposited at 210 °C. The data exhibit a fast initial decay followed by a slower decay at longer time. The solid curve shows that Eq. (1), which describes two exponential decay processes, provides a good fit to the data. Inset: Multiple in-plane $(H,K)_H$ reflections show approximately the same rate of intensity decay, indicating the loss of the 7×7 surface fraction with time.

shown in Fig. 6. The data show a decay rate that is significantly faster during an initial decay period (∽10 min) than at later times, suggesting that there are two time regimes. The time-dependent data fit well to a sum of two exponentials

$$I(t) = I_1 e^{-\frac{t}{\tau_1}} + I_2 e^{-\frac{t}{\tau_2}}, \tag{1}$$

where $I_j$'s are scale constants and the $\tau_j$'s are the time constants. A fit of the data to Eq. (1) is shown in Fig. 6. Although we can not address the physical origin of the two time constants from the present data alone, the form of the decay suggests a two-step process that occurs sequentially in time (an intermediate structure may also be involved).

The time-dependent decay of the intensity, such as that shown in Fig. 6, was measured at different temperatures from which an estimate of the activation energy could be obtained for the destruction of the Si(111)7×7 covered with a monolayer of Pb. The logarithm of the two time constants obtained from a fit of the data to Eq. (1) is plotted versus inverse temperature in Fig. 7. $I_1$ and $I_2$ were found to be reasonably constant (to within ±12%) with temperature, so that only $\tau_1$ and $\tau_2$ are temperature dependent, giving further support to the notion that Eq. (1) represents a two-step decay process. The activation energy $E_b$ and attempt frequency $\nu$ for both time constants were extracted from an Arrhenius law according to

$$\ln(\tau) = \frac{E_b}{k_B T} - \ln(\nu). \tag{2}$$

The results for both time constants are shown in Table I and by the lines in Fig. 7. It is noted that the slowest process corresponds to the smaller of the two activation energies.

A similar analysis was used to estimate an activation energy barrier for the low-temperature annealing regime using the *increasing intensity* data in Fig. 1. Because these lower-

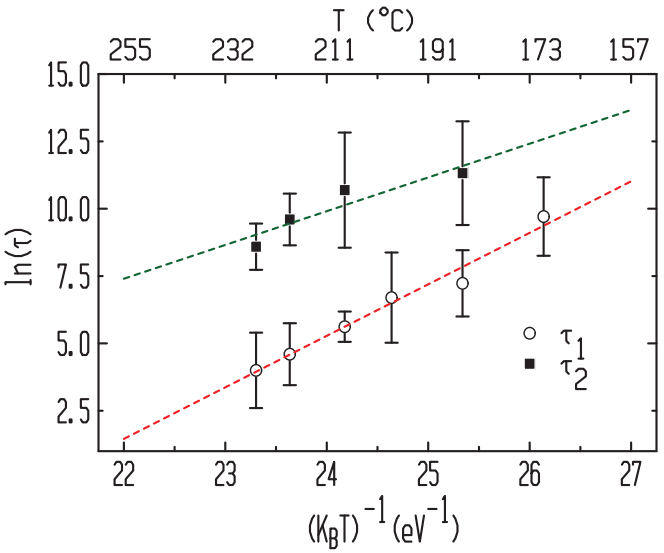


FIG. 7. (Color online) $\ln(\tau)$ for both time constants $\tau_1$ and $\tau_2$ as a function of inverse temperature was obtained from fits of Eq. (1) to the time decay of the $(\frac{8}{7},0)_H$ intensity at different annealing temperatures. The $\tau$'s are measured in seconds. Two temperatures do not have $\tau_2$ values because there was insufficient time data. The dashed lines represent fits to each set of time constants according to the Arrhenius behavior given in Eq. (2).

TABLE I. Activation energy $E_b$ and attempt frequency $\nu$, obtained from fitting Eq. (2) to the data in Fig. 7.

| | $\tau_1$ | $\tau_2$ |
|---|---|---|
| $E_b$ | 1.9(±0.2) eV | 1.3(±0.2) eV |
| $\nu$ | $4 \times 10^{17(\pm 3)}$ Hz | $6 \times 10^{8(\pm 3)}$ Hz |

temperature data are more limited compared to our high-temperature studies, a barrier from only a single time constant was determined: $\tau_1$ is 600(±60) s at 47 °C and 150(±15) s at 77 °C, from which we estimate the activation energy barrier for the low-temperature annealing of the Pb8×8 to be $E_b = 0.4(\pm 0.2)$ eV, with attempt frequency $\nu = 2 \times 10^{4(\pm 1)}$ Hz. This barrier is more than three times smaller than for the activation energy determined at higher temperature for the decaying intensities.

The measured energy barriers can be compared to various atomic-scale processes that have been discussed in the literature. For example, Pb adatom diffusion on the wetting layer and on top of a QSE Pb island have barriers of 0.1 and 0.05 eV, respectively.[17] These values are significantly smaller than the 0.4-eV barrier that we measured during the low-temperature annealing. However, rather than simple diffusion across a surface, our diffraction data in the low-temperature regime show that the Pb atoms rearrange within the unit cell, suggesting that atoms move in and out of the wetting layer and/or possibly move within it. Modeling of recent low-energy electron microscopy (LEEM) experiments have suggested a barrier for the mobility of the Pb wetting layer to be 0.2–0.36 eV.[18] This is close to our measured value and it gives additional evidence that the low-temperature annealing observed in our experiment arises from an atomic-scale structural rearrangement of the wetting layer. Turning now to the higher-temperature regime, our measurements show a much larger energy barrier that is in the range of 1.3–1.9 eV. Since our measurements show that this annealing regime destroys the underlying Si(111)7×7, having a larger energy barrier is reasonable as it will involve complex motions of both Pb and Si. To our knowledge, an energy barrier for destroying the 7×7 in the presence of a metal layer has not been previously measured. However, the energy barrier for desorption of Pb is known to be in the range 2.31–2.64 eV,[12,19] and this can be taken as an upper limit. The barrier that we measured at high temperature is considerably less than this, but much larger than the mobility barrier of the wetting layer.

Our studies also reveal that the high-temperature decay of the Pb/Si(111)7×7 depends on the Pb coverage. Figure 8 shows the decaying $(\frac{8}{7},0)_H$ intensity with elapsed time for three different coverages that were deposited at 185 °C. As can be seen, there is an increase in the decay *rate* in going from 1.2 to 1.5 ML coverage; this is quantitatively shown in the inset where the relaxation time decreases with coverage. In considering the 2.5-ML data in Fig. 8, it should be noted that the *initial* $(\frac{8}{7},0)_H$ intensity decreases with increasing coverage above 1.2 ML because the Pb nanocrystalline islands consume the wetting layer directly below the islands and incorporate that Pb into the fcc structure of the islands, as has been reported elsewhere.[11,21] Thus, the lower intensity for the 2.5-ML data in Fig. 8 is at least partly due to this effect.

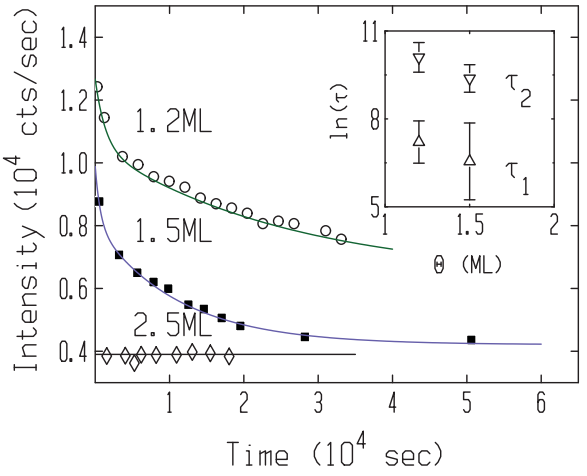


FIG. 8. (Color online) The decay of the $(\frac{8}{7},0)_H$ peak intensity with elapsed time after the deposition of a given coverage of Pb at 185 °C. Note that the intensity decays more quickly for 1.5 ML than for 1.2 ML. There is no decay observed for 2.5 ML. The solid curves are calculated from Eq. (1), which was fit to the data. The inset shows the time constants vs coverage for the fitted curves.

However, at a coverage of 2.5 ML, there is no discernible decay of the intensity with time at this temperature. Therefore, we can not say whether the 2.5-ML data decays faster or slower than the experimental measurement time, although, extending the trend from lower coverage would suggest that it decays faster. The result of Fig. 8 bears similarity to recent LEEM experiments on Pb/Si(111) (Ref. 18) that have shown anomalous kinetic behavior of the Pb wetting layer in response to a hole generated by a short-pulsed laser. Those experiments showed that the Pb relaxation rate $\frac{1}{\tau}$ increased with increasing coverage between 1.2 and 1.3 ML, with no change in relaxation rate at higher coverages. Some care in making a comparison between the two experiments should be exercised, however, since the activation energies differ by almost an order of magnitude. The higher activation energy in the present experiment is likely to be related to the motion of the Si adatoms that is required to remove the 7×7 reconstruction.

## IV. CONCLUSIONS

These experiments demonstrate that there are two unrelated and physically distinct mechanisms by which the Pb/Si(111)7×7 wetting layer is not in equilibrium. One mechanism derives from the fact that the wetting layer is irreversibly metastable because the Si(111)7×7 reconstructed surface is no longer stable once the metal is deposited on it. However, the second mechanism relates to the structure of the Pb wetting layer itself. When Pb is deposited at low temperature, the disordered atomic-scale structure anneals, by time and/or temperature, and the ordering in the wetting layer improves. This suggests that there would be an equilibrium structure of the wetting layer if the Si(111)7×7 were static and not subject to the first instability mechanism. Apparently, the wetting layer does not easily adapt to the highly corrugated surface of the Si(111)7×7 so that there is a slow approach (requiring annealing) to the equilibrium structure. Together, the two mechanisms lead to a broad temperature range (more

than 200 °C) over which the wetting layer structure is observed to change with time.

Finally, we discuss potential implications of these results for the growth and coarsening of QSE islands that form on the wetting layer. A subtle but important point for kinetic considerations is that the as-grown wetting-layer structure is not simply disordered as its native state, which has been the prevailing view. Instead, the wetting layer is disordered as a result of not having attained its equilibrium structure. Therefore, adatoms moving across the wetting layer can encounter a dynamic energy landscape: the *unstable* wetting layer atoms might react to the adatoms, leading to a complex adatom mobility. Second, the growth and coarsening of QSE islands could depend on how the wetting layer was prepared, because our results demonstrate that the structure of the wetting layer depends on both the growth and annealing temperatures as well as the annealing time. Therefore, even though the QSE islands are grown at temperatures lower (typically below or near −50 °C) than the temperatures used in this paper, the structural foundation for growing the QSE islands is set by the preparation steps used in creating the wetting layer, which we have now shown does not have a unique structure. Although the degree to which these effects influence the growth and coarsening of the QSE islands is not presently known, the wetting layer is, nevertheless, both the conduit for mass transport between the islands and it is the template upon which the islands form. Therefore, the nonequilibrium behavior of the wetting layer revealed in this paper must be an important consideration for understanding the role of the wetting layer in the growth and coarsening of QSE islands.

## ACKNOWLEDGMENTS

Research funding is gratefully acknowledged from the National Science Foundation, Grant No. DMR0706278 (M.W.G., S.T.H., Y.C., P.F.M.), the Industrial Source Technology Development Programs (2009-F014-01) of the Ministry of Knowledge Economy (MKE) of Korea (CK), and Canim Scientific (EHC). The Advanced Photon Source is supported by the DOE Office of Basic Energy Sciences, Contract No. W-31-109-Eng-38. The 6IDC beam line is supported through the Ames Lab, operated for the US DOE by Iowa State University under Contract No.W-7405-Eng-82.

[1]F. K. Schulte, Surf. Sci. **55**, 427 (1976); P. J. Feibelman, Phys. Rev. B **27**, 1991 (1983).

[2]Z. Zhang, Q. Niu, and C-K. Shih, Phys. Rev. Lett. **80**, 5381 (1998).

[3]K. Budde, E. Abram, V. Yeh, and M. C. Tringides, Phys. Rev. B **61**, R10602 (2000).

[4]J. W. Evans, P. A. Thiel, and M. C. Bartelt, Surf. Sci. Rep. **61**, 1 (2006).

[5]C. A. Jeffrey, E. H. Conrad, R. Feng, M. Hupalo, C. Kim, P. J. Ryan, P. F. Miceli, and M. C. Tringides, Phys. Rev. Lett. **96**, 106105 (2006).

[6]M. Hupalo, S. Kremmer, V. Yeh, L. Berbil-Bautista, E. Abram, and M. C. Tringides, Surf. Sci. **493**, 526 (2001).

[7]F. Grey, R. Feidenhans'l, M. Nielsen, and R. L. Johnson, J. Phys. (Paris) **50**, 7181R (1989); R. Feidenhans'l, F. Grey, M. Nielson, and R. L. Johnson, in *Kinetics of Ordering and Growth at Surfaces*, edited by M. G. Lagally (Plenum Press, New York, 1990).

[8]E. Ganz, I. Hwang, F. Xiong, S. K. Theiss, and J. Golovchenko, Surf. Sci. **257**, 259 (1991).

[9]I. Hwang, R. E. Martinez, C. Liu, and J. Golovchenko, Surf. Sci. **323**, 241 (1993).

[10]C. A. Jeffrey, R. Feng, E. H. Conrad, P. F. Miceli, C. Kim, M. Hupalo, M. C. Tringides, and P. J. Ryan, Superlattices Microstruct. **41**, 168 (2007).

[11]R. Feng, E. H. Conrad, M. C. Tringides, C. Kim, and P. F. Miceli, Appl. Phys. Lett. **85**, 3866 (2004).

[12]G. Le Lay, J. Peretti, M. Hanbucken, and W. S. Yang, Surf. Sci. **204**, 57 (1988).

[13]C. Kumpf, O. Bunk, J. H. Zeysing, M. M. Nielsen, M. Nielsen, R. L. Johnson, and R. Feidenhansl, Surf. Sci. **448**, L213 (2000).

[14]K. Horikoshi, X. Tong, T. Nagao, and S. Hasegawa, Phys. Rev. B **60**, 13287 (1999).

[15]S. Stepanovsky, M. Yates, V. Yeh, M. Hupalo, and M. C. Tringides, Surf. Sci. **600**, 1417 (2006).

[16]K. A. Edwards, P. B. Howes, J. E. MacDonald, T. Hibma, T. Bootsma, and M. A. James, Surf. Sci. **424**, 169 (1999).

[17]M. Hupalo and M. C. Tringides, Phys. Rev. B **75**, 235443 (2007); Z. Kuntova, M. Hupalo, Z. Chvoj, and M. C. Tringides, *ibid.* **75**, 205436 (2007).

[18]K. L. Man, M. C. Tringides, M. M. T. Loy, and M. S. Altman, Phys. Rev. Lett. **101**, 226102 (2008).

[19]M. Saitoh, K. Oura, K. Asano, F. Shoji, and T. Hanawa, Surf. Sci. **154**, 394 (1985).

[20]M. Hupalo, V. Yeh, L. Berbil-Bautista, S. Kremmer, E. Abram, and M. C. Tringides, Phys. Rev. B **64**, 155307 (2001).

[21]M. W. Gramlich, S. T. Hayden, C. A. Jeffrey, C. Kim, R. Feng, E. H. Conrad, and P. F. Miceli, Metall. Mater. Trans. A **41**, 1159 (2010).